Catalysis Science & Technology

PAPER

View Article Online
View Journal | View Issue

Cite this: *Catal. Sci. Technol.*, 2018, **8**, 344

Dynamic equilibria in supported ionic liquid phase (SILP) catalysis: *in situ* IR spectroscopy identifies $[Ru(CO)_xCl_y]_n$ species in water gas shift catalysis†

Tanja Bauer,[a] Robert Stepic,[b] Patrick Wolf,[c] Fabian Kollhoff,[a] Weronika Karawacka,[a] Christian R. Wick,[d] Marco Haumann,[c] Peter Wasserscheid,[cf] David M. Smith,[de] Ana-Sunčana Smith[b] and Jörg Libuda*[af]

Received 26th October 2017,
Accepted 27th November 2017

DOI: 10.1039/c7cy02199b

rsc.li/catalysis

Ru-based supported ionic liquid phase (SILP) systems efficiently catalyze the low-temperature water-gas shift reaction (WGSR). While previous studies suggest that Ru-carbonyl species play an important role in the mechanism, detailed knowledge on the catalytically active species is still missing. To identify these carbonyl complexes, we apply *in situ* diffuse reflectance infrared Fourier transform spectroscopy (DRIFTS) in combination with density functional theory (DFT). Investigations of an as-prepared $[Ru(CO)_3Cl_2]_2$/$[C_4C_1C_1Im]Cl/Al_2O_3$ catalyst indicate splitting of the dimer induced by Cl^-. Subsequently, an equilibrium between several $[Ru(CO)_xCl_y]_n$ species is established, in which the IL serves as an effectively infinite Cl^- reservoir. We find that the major species in the system freshly-prepared from $[Ru(CO)_3Cl_2]_2$ is indeed $[Ru(CO)_3Cl_3]^-$. A smaller amount of $[Ru(CO)_2Cl_3]^-$ and chloride-rich species $[Ru(CO)_2Cl_4]^{2-}$ or $[RuCOCl_4]^{2-}$ are also found in the SILP. Similar Ru-carbonyl species are observed during carbonylation of $RuCl_3$/$[C_4C_1C_1Im]Cl/Al_2O_3$, another potential WGSR catalyst. The response of $[Ru(CO)_3Cl_2]_2/[C_4C_1C_1Im]Cl/Al_2O_3$ to heating and/or CO dosing was probed *in situ* and the results confirm the presence of the equilibrium proposed above.

1. Introduction

The increasing importance of hydrogen-based technologies leads to an increasing demand for H_2 production from hydrocarbon sources such as syngas and methanol, which may serve as energy storage media.[1–2] To maximize the H_2 release from these sources, one important step is the water-gas shift reaction (WGSR), *i.e.* the exothermic conversion of CO and H_2O to CO_2 and H_2, which decreases the amount of CO and increases the H_2 concentration in the product gas.[1–3] Ru-based systems, especially Ru-carbonyls, are common catalysts to promote the WGSR at low temperature, where the forward reaction is thermodynamically favored.[1,3,4] Werner *et al.* screened a series of homogeneous Ru catalysts in supported ionic liquid phase (SILP) systems.[5] In this study, the SILP concept is applied to immobilize the active catalyst on a porous support using a thin coating of ionic liquid (IL).[6,7] The negligible vapor pressure of ILs prevents stripping of the IL layer and leads to a very high long-term stability of the SILP catalysts.[6–8] In their work, the authors showed that a SILP system prepared from the simple $RuCl_3$ precursor, with 1-butyl-2,3-dimethylimidazolium trifluoromethanesulfonate ($[C_4C_1C_1Im][OTf]$) as the IL, formed the most active catalyst. However, the full activity of this system was only reached after an induction period of approximately 60 h.[9]

Interestingly, spectroscopic *ex situ* analysis of a used $RuCl_3/[C_4C_1C_1Im][OTf]/Al_2O_3$ sample indicated the presence of Ru-carbonyl species. This finding suggests that new $[Ru(CO)_xCl_y]_n$ complexes with enhanced catalytic activity are formed during the induction period of the WGS reaction itself.[9] Indeed, the desired activity and selectivity was achieved without an induction period when $[Ru(CO)_3Cl_2]_2/[C_4C_1C_1Im][OTf]/Al_2O_3$ was used as a catalyst.[10] However, these studies did not reveal the exact nature of the catalytically active carbonyl complex. Thus, the following questions

[a] *Lehrstuhl für Physikalische Chemie II, Friedrich-Alexander-Universität Erlangen-Nürnberg, Egerlandstraße 3, D-91058 Erlangen, Germany. E-mail: joerg.libuda@fau.de*
[b] *PULS Gruppe, Lehrstuhl für Theoretische Physik I, Friedrich-Alexander-Universität Erlangen-Nürnberg, Nägelsbachstraße 49b, D-91052 Erlangen, Germany*
[c] *Lehrstuhl für Chemische Reaktionstechnik, Friedrich-Alexander-Universität Erlangen-Nürnberg, Egerlandstraße 3, D-91058 Erlangen, Germany*
[d] *Ruđer Bošković Institute, Bijenička cesta 54, P.P. 180, HR-10002 Zagreb, Croatia*
[e] *Computer Chemie Centrum, Friedrich-Alexander-Universität Erlangen-Nürnberg, Nägelsbachstraße 25, 91052 Erlangen, Germany*
[f] *Erlangen Catalysis Resource Center and Interdisciplinary Center Interface-Controlled Processes, Friedrich-Alexander-Universität Erlangen-Nürnberg, 91058 Erlangen, Germany*

† Electronic supplementary information (ESI) available. See DOI: 10.1039/c7cy02199b

still remain unanswered to date: a) what is the exact nature and concentration of the carbonyl species present in the SILP WGSR system? b) Which of the present species shows the highest catalytic activity (in terms of TON and TOF)? It is obvious that only if the most active carbonyl complex is also the most abundant one in the SILP system under reaction conditions, the activity of the resulting SILP catalyst system it at its maximum.

The present study addresses mainly the first question and elucidates the existence and amount of different $[Ru(CO)_xCl_y]_n$ species in two representative SILP systems: $RuCl_3/[C_4C_1C_1Im]Cl/Al_2O_3$ and $[Ru(CO)_3Cl_2]_2/[C_4C_1C_1Im]Cl/Al_2O_3$. For this purpose, we use *in situ* infrared (IR) spectroscopy, a particularly powerful tool in metal carbonyl chemistry. In combination with density functional theory (DFT) calculations, this approach allows us to identify the nature of the carbonyl complexes by careful analysis of the CO stretching frequency region. Previously, even the nature of intermediates could be identified by transient IR spectroscopy.[11] In this work, we aim at a detailed understanding of the species which are present during the reaction. In contrast to earlier studies,[10] we utilize here 1-butyl-2,3-dimethylimidazolium chloride ($[C_4C_1C_1Im]Cl$) as the IL, because the enhanced chloride content has been shown to further enhance the activity. In particular, we focus on the influence of the IL upon preparation of the active catalyst, as well as on the effects of temperature and CO on the speciation in the active catalysts.

2. Experimental procedures, setups and materials

2.1. Reactor setup for infrared measurements

All IR experiments were performed using a Bruker Vertex 80v FTIR spectrometer with KBr beam splitter and a liquid nitrogen cooled mercury–cadmium–telluride (LN-MCT) detector.

Transmission infrared spectroscopy (TIRS) measurements were either conducted with KBr pellets or using a KBr window as IR transparent support. The solutions were drop-cast onto a KBr window which, after evaporation of the solvent, was mounted in the sample compartment on a sample holder (Pike). Evacuation of the sample compartment leads to complete removal of the solvent. The acquisition time for TIR spectra was 1 min with a spectral resolution of 2 cm^{-1}.

All diffuse reflectance infrared Fourier transform spectroscopy (DRIFTS) experiments were carried out in a home-built reactor system, which is described in detail elsewhere.[12] Briefly, a high temperature reactor chamber and praying mantis diffuse reflectance accessory (both from Harrick) are placed in the sample compartment of the spectrometer. A home-built extension of the sample compartment, equipped with all necessary electrical and gas dosing feedthroughs, allows for keeping the complete optical path evacuated during the measurements. This maximizes the stability of the system, especially for long-term experiments. The reactor is equipped with CaF_2 windows and a type K thermocouple directly contacting the examined sample, which provides excellent temperature control. Currently, the setup can be operated at pressures adjustable from 1 mbar to 20 bar using three pressure controllers (PCs). Up to five different gases can be dosed *via* mass flow controllers (Bronkhorst, MFCs). The setup can be operated in an automated way, which allows accurate programming of temperature, pressure and gas composition. In the CO (Linde, 4.7) dosing experiments the gas dosing (30 min, 1 bar, 20 mL_N min^{-1}) was followed by evacuation to 1 mbar for 1 min and, finally, by purging with Ar (Linde 5.0, 15 min, 1 bar, 20 mL_N min^{-1}) at 1 bar. The two last steps result in efficient removal of the CO gas phase from the reactor. This procedure was carried out repeatedly, if required, at different temperatures. All DRIFT spectra were recorded using an acquisition time of 5 min and a spectral resolution of 2 cm^{-1}.

2.2. Preparation of the SILP systems

A typical SILP catalyst is made from a metal complex which is dissolved in an IL and, subsequently, dispersed onto the surface of a porous solid support. For the current study aluminum oxide (γ-Al_2O_3) was used as a support, which was purchased from Sasol Germany GmbH (LOT: B39598) and sieved to a fraction of 200 μm < dP < 500 μm. $[Ru(CO)_3Cl_2]_2$ which was used as precursor complex was purchased from Alfa Aesar (LOT: T20C0136B). Two ILs were used, $[C_4C_1C_1Im]Cl$ and $[C_4C_1C_1Im][OTf]$, which were purchased from Merck KGaA (LOT: 99/818 and LOT: 99/902 respectively). The SILP materials were prepared with high purity dichloromethane (DCM) as solvent in the preparation procedure (Sigma-Aldrich, LOT: SZBG073AV). $RuCl_3$ was purchased from Sigma Aldrich (LOT: MKBH0927V).

In a first step, $[C_4C_1C_1Im]Cl$ was dissolved in high purity DCM (typically 30 mL) in a round-bottom Schlenk flask under Ar atmosphere. After stirring till complete dissolution of the IL (10–15 min at 25 °C), the Ru catalyst (either $RuCl_3$ or $[Ru(CO)_2Cl_3]_2$) was added followed by another stirring for 10 min. Subsequently, the γ-Al_2O_3 support was added and stirred quickly for 2–5 min. To avoid crushing of the particles due to mechanical stress, the stirrer bar was taken out before removal of the solvent in two steps (step 1: 3 h, 40 °C, 900 mbar; step 2: 1 h, 40 °C, <3 mbar) in a rotary evaporator. After solvent removal, free flowing SILP catalyst particles were obtained. The resulting catalyst has a Ru loading of w_{Ru} = 0.04 g_{RU} $g_{support}^{-1}$ while the pore filling grade with IL is α = 0.34. The pore filling grade describes the IL volume related to the total pore volume of the support material (V_{IL} $V_{support}^{-1}$).

2.3. Computational details

The DFT calculations were carried out using the TURBOMOLE[13,14] software package. The BP86[15,16] functional was used in combination with the def2-TZVPP[17] basis set, which was augmented by diffuse functions for C, Cl, H and O atoms taken from the aug-cc-PVTZ[18,19] basis set. This

approach has been successfully applied to similar systems.[20] Optimizations were carried out without any constraints and vibrational frequencies were determined using the analytical derivatives of the energy as implemented in the AOFORCE module within TURBOMOLE.

3. Results and discussion

In the following, experimentally observed spectral features are mainly compared to the respective DFT results. For sake of clarity, a complete summary and comparison of DFT and experimental spectra of all Ru-species is given in Table 1.

3.1. Influence of the IL on $[Ru(CO)_3Cl_2]_2$ during catalyst preparation

The TIR spectrum of a freshly-prepared SILP catalyst in a KBr disc is shown in Fig. 1a. The spectrum can be divided into regions dominated by IL features (<1600 cm^{-1} and >2500 cm^{-1}) and carbonyl features from the Ru-species (2200–1700 cm^{-1}). The spectral region below ~1000 cm^{-1} cannot be probed due to total absorption of Al_2O_3.[21] $[C_4C_1C_1Im]Cl$ gives rise to asymmetric and symmetric C–H stretching features ν_{as}/ν_s at 3115, 2963 and 2875 cm^{-1}, respectively.[22] Furthermore, peaks in the fingerprint region can be assigned to C–N stretching ν (1588 and 1540 cm^{-1}), C–H rocking δ_{as} (1540 and 1254 cm^{-1}) and C–H scissor δ_s (1469 and 1422 cm^{-1}) vibrations.[22] The carbonyl region shows very intense C–O stretching features corresponding to CO-ligands of $[Ru(CO)_xCl_y]_n$. Strikingly, the CO-features at 2033 and 1951 cm^{-1} obtained from the $[Ru(CO)_3Cl_2]_2/[C_4C_1C_1Im]Cl/Al_2O_3$ SILP system differ strongly from what was found by us and others in previous studies with $[Ru(CO)_3Cl_2]_2$ in other Cl-free ILs.[20,23,24] We attribute the occurrence of the new peaks to a transformation of the Ru complex in the chloride IL phase. The most likely scenario is a splitting of the dimer by addition of Cl^- and formation of $[Ru(CO)_3Cl_3]^-$, a reaction which was proven previously by experimental and theoretical studies.[25] Furthermore, the calculated IR spectrum of the energetically favorable facial (*fac*-)$[Ru(CO)_3Cl_3]^-$ isomer fits the experimentally obtained peaks well (see Table 1). With respect to this finding, the IL may be regarded as an "infinite" reservoir of Cl^- ligands. Dimer splitting was previously also observed in an ion-free environment by Motterlini *et al.*, who showed that, in DMSO, solvent molecules may serve as ligands as well, breaking the dimer into di- and tricarbonyl monomers.[26]

To further prove this hypothesis, we prepared $[C_4C_1C_1Im]Cl:[Ru(CO)_3Cl_2]_2$ mixtures (weight ratio 2:1 and 5:1) in DCM. The TIRS spectra are displayed in Fig. 1b. All spectra are normalized to the peak at 2030–2040 cm^{-1}, therefore no scale bar is given. The freshly prepared 2:1 mixture (black curve) shows two features at 2122 and 2043 cm^{-1}. Based on our DFT calculation we attribute these peaks to intact $[Ru(CO)_3Cl_2]_2$.[23,26] Previously, Tsuchiya *et al.* assigned these peaks to $[Ru(CO)_3Cl_3]^-$,[25] which, however, would not agree with our present DFT data. The more pronounced red-shift with respect to previously published IRAS data is attributed to the solvent effects due to the increased amount of IL.[20] With increasing IL concentration in the 5:1 mixture (red curve), a small feature appears at 1950 cm^{-1} and the intensity of the peak at 2122 cm^{-1} decreases. Presumably, part of the $[Ru(CO)_3Cl_2]_2$ dimer is at this stage already converted to $[Ru(CO)_3Cl_3]^-$. The spectrum taken of the 5:1 mixture after 5 days (blue curve) follows this trend. No peak can be seen at 2122 cm^{-1}, which indicates that the dimer species is completely consumed. In addition to the expected features of $[Ru(CO)_3Cl_3]^-$ (2032 and 1950 cm^{-1}) a new peak is visible at 1908 cm^{-1}. It most likely corresponds to chloride-rich, di-anionic species like, *i.e.*, $[Ru(CO)_2Cl_4]^{2-}$ or $[Ru(CO)Cl_4]^{2-}$, which are formed by further CO/Cl^- ligand-exchange reactions. Comparison with DFT data shows that the peak matches very well the calculated position for *trans*-$[Ru(CO)_2Cl_4]^{2-}$, but this complex is energetically unfavorable (88 kJ mol^{-1}). Its corresponding *cis*-isomer on the other hand should lead to two peaks. The calculated spectrum of $[RuCOCl_4]^{2-}$ shows a single peak (1862 cm^{-1}) and could therefore also be responsible for the feature at 1908 cm^{-1}. This would then mean that a direct ligand substitution reaction

Table 1 Comparison of experimentally and calculated IR peaks, the most intense peaks are marked in bold

Ru species	Configuration	Peak center DFT [cm^{-1}]	Peak center exp. [cm^{-1}]	Δ(DFT–exp) [cm^{-1}]	E_{rel} [kJ mol^{-1}]
$[Ru^{II}(CO)_3Cl_2]_2$	*trans*	2107, 2040	2122, ~**2045**	−15, −**5**	0
$[Ru^{II}(CO)_3Cl_2]$	s.-pyr. *cis*	2101, **2033** + **2025**	**2122**, 2055	−**21**, −26	0
$[Ru^{II}(CO)_3Cl_2]$	s.-pyr. *trans*	**2054**, 2015	**2040**, 2002	**14**, 13	44
$[Ru^{II}(CO)_3Cl_3]^-$	facial	2063, **1983**	~2030, ~**1950**	~33, ~**33**	0
$[Ru^{II}(CO)_3Cl_3]^-$	meridial	1972, **2003**, 2091	—	—	39
$[Ru^{II}(CO)_2Cl_3]^-$	s.-pyr. *cis*	2010, **1939**	2008, 1922	2, 17	0
$[Ru^{II}(CO)_2Cl_3]^-$	s.-pyr. *trans*	1943	—	—	123
$[Ru^{II}(CO)_2Cl_4]^{2-}$	*cis*	1969, **1893**	—, ~**1900**	—, ~−7	0
$[Ru^{II}(CO)_2Cl_4]^{2-}$	*trans*	1894	~1900	~6	88
$[Ru^{II}COCl_4]^{2-}$	s.-pyr.	1862	~1900	~38	
$[Ru^{II}(CO)_4Cl_2]$	*cis*	(2149), **2086** + 2066, 2035	2140, **2078**, —	9, **8**, —	0
$[Ru^{II}(CO)_4Cl_2]$	*trans*	2060	—	—	40
$[Ru^{0}(CO)_3Cl_2]^{2-}$	trig.-bipyr. *cis*	1910, 1803, **1787**	—	—	25
$[Ru^{0}(CO)_3Cl_2]^{2-}$	trig.-bipyr. *trans*	1777	—	—	0
$[Ru^{II}(CO)_2(CO–OH)HCl_3]$		2025, 1953, **1704**, 1678	(1780/1730)	—	42
$[Ru^{II}(CO)_2(CO–OH)Cl_2]$ + HCl		**2117**, 2013, 1944, 1728	—	—	0

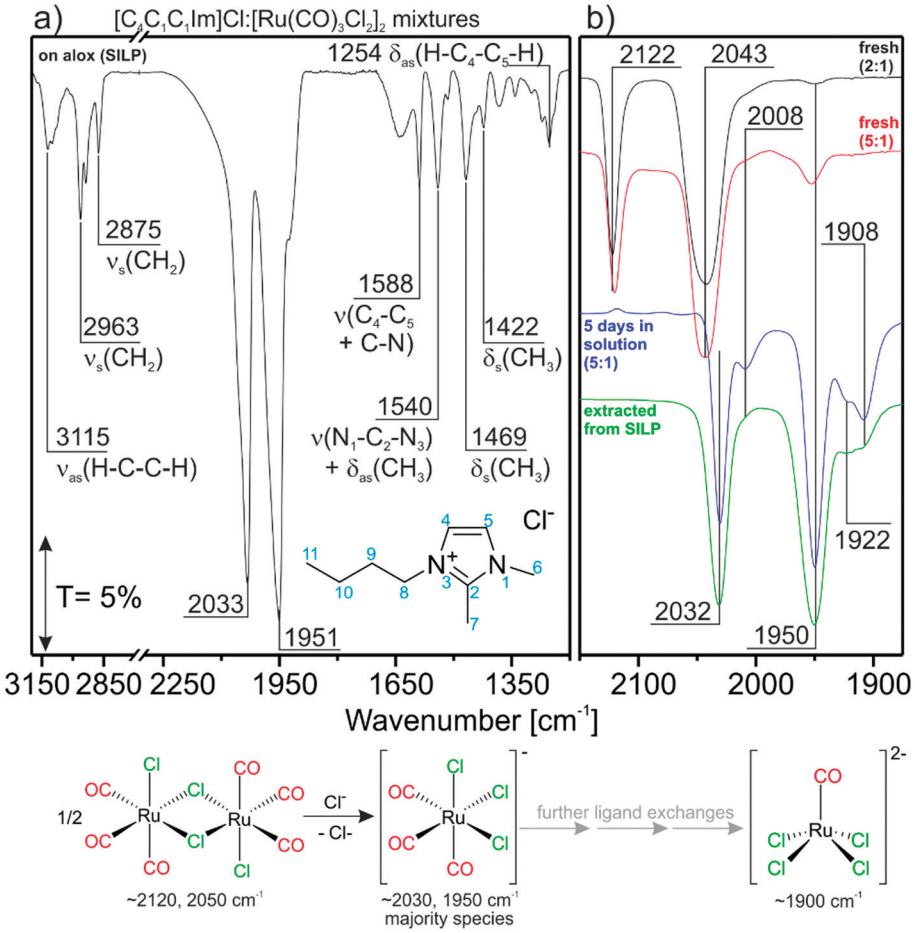

Fig. 1 Reference TIR spectra for; a) the as-obtained $[Ru(CO)_3Cl_2]_2/[C_4C_1C_1Im]Cl/Al_2O_3$ SILP system. The assignment is given for IL bands; b) $[Ru(CO)_3Cl_2]_2/[C_4C_1C_1Im]Cl$ mixtures prepared with DCM.

from $[Ru(CO)_2Cl_3]^-$ to $[RuCOCl_4]^{2-}$ takes place. Although no unambiguous assignment of all features can be made at the moment, we summarize that chloride-rich $[Ru(CO)_2Cl_4]^{2-}$ or $[RuCOCl_4]^{2-}$ di-anions are formed from the dimer by sequential ligand substitution reactions. The two small features at 2008 and 1922 cm^{-1} can be assigned to an intermediate species *cis*-$[Ru(CO)_2Cl_3]^-$.

For comparison, we extracted the Ru-species also from the fresh catalyst using DCM. The corresponding TIR spectra are included in Fig. 1b (in green). As expected, the spectrum obtained is similar to both the TIR spectra of the "intact" SILP (Fig. 1a) and the one obtained from the 5 : 1 mixture after 5 days in solution. This proves that the Cl^--induced splitting of the Ru-dimer observed without support material in solution also takes place during preparation of the SILP catalyst. We assume that the formation of monomers is a function of the IL concentration and time. As shown by the spectra of the catalyst after extraction, the Ru-carbonyls can be completely removed from the as-prepared SILP with the non-ligating solvent DCM. Therefore, one can conclude that all species are physically dissolved in the IL phase in the system.[23]

More detailed insight into the conversion of the dimer species to a variety of monomers in the chloride-containing IL can be gained by studying the transformation *in situ*. To this end, the 2 : 1 $[C_4C_1C_1Im]Cl:[Ru(CO)_3Cl_2]_2$ mixture was deposited on a KBr window and IR spectra were taken *in vacuo* every 30 min (~1 mbar, air). The results are displayed in Fig. 2. As the features at 2047 and 2036 cm^{-1} lie quite close, they cannot be resolved for integration. The peak assigned to the dimer at 2121 cm^{-1} decreases linearly in time, while the peak related to $[Ru(CO)_3Cl_3]^-$ at 1951 cm^{-1} increases simultaneously. The integrated peak areas of the intermediate species $[Ru(CO)_2Cl_3]^-$ with peaks at 2009 and 1919 cm^{-1} increase more steeply in the first 480 min indicating that this complex forms more rapidly at the beginning. As previously observed, its amount is rather small throughout the experiment. The experiment shows the first stage of dimer splitting, therefore, no peak related to the di-anionic species is observed.

In order to prove that Cl^- ions in the IL are responsible for the transformation of the dimer, we repeated the TIRS measurements with IL solutions providing lower Cl^- concentration. First, a 1 : 1.2 mixture of $[C_4C_1C_1Im][OTf]$ and $[C_4C_1C_1Im]Cl$ was applied to prepare the solutions as described above. Second $[C_4C_1C_1Im][OTf]$ with no additional Cl^-, apart from the intrinsic amount from $[Ru(CO)_3Cl_2]_2$ was

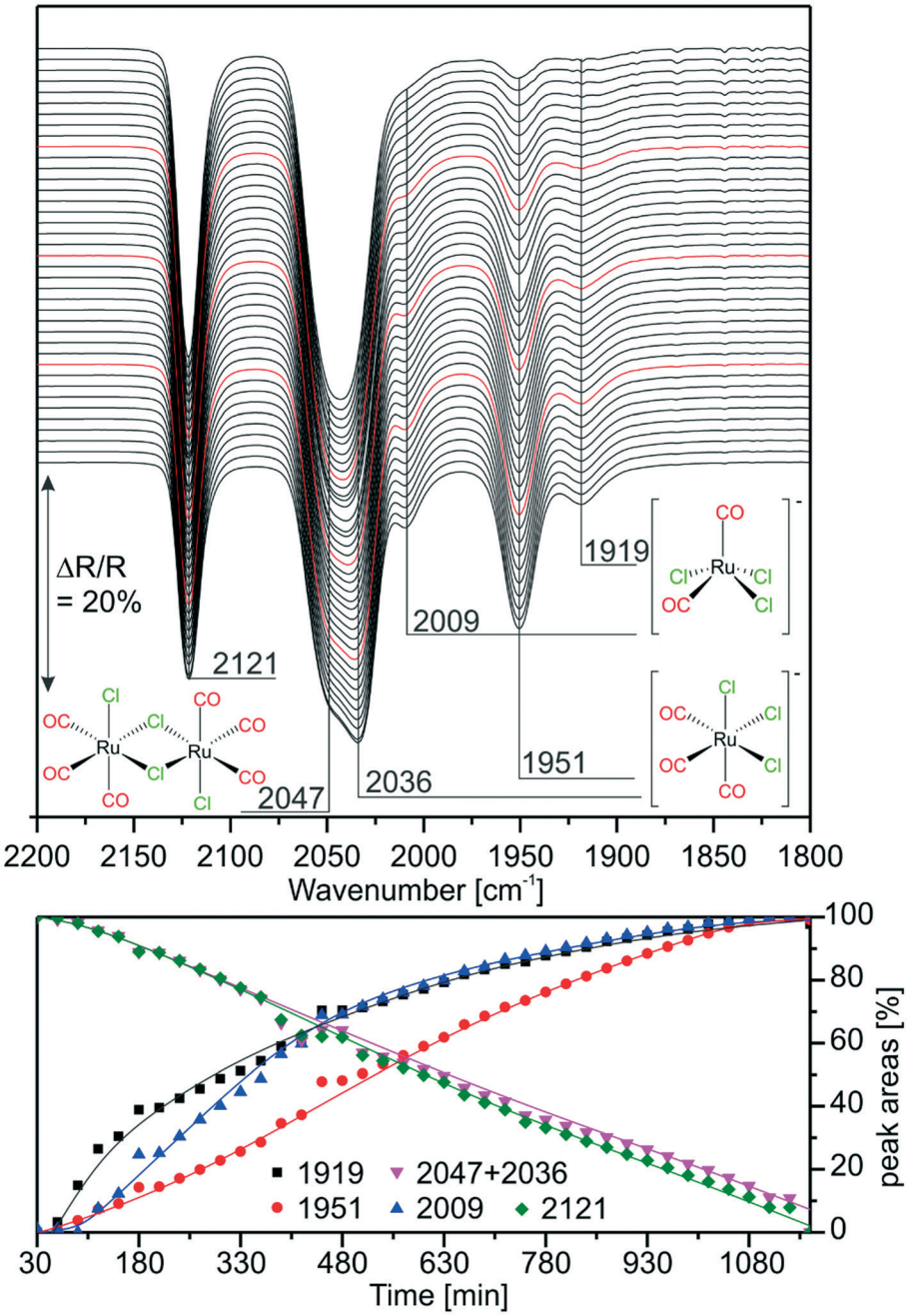

Fig. 2 Top: Offset, time-resolved transmission spectra of a $[Ru(CO)_3Cl_2]_2$: $[C_4C_1C_1Im]Cl$ (1 : 2) mixture deposited on a KBr window taken every 30 min in vacuum; bottom: normalized peak areas (all lines are guides to the eye).

used. In contrast to the pure Cl^- containing IL, the spectrum of the $[OTf]^-/Cl^-$ mixture after 5 days (see Fig. 3a) shows a peak at 2125 cm^{-1} indicating that the dimer is indeed only partly split. In the spectra obtained from the pure $[C_4C_1C_1Im][OTf]$ solution no monomer peak at 1950 cm^{-1} is formed and the peaks of the dimer species around 2130 and 2056 cm^{-1} are present even after 5 days (see Fig. 3b). This proves that a smaller Cl^- content is associated with a higher amount of intact dimer in the DCM solution. In the case of a chloride-free IL no transformation of $[Ru(CO)_3Cl_2]_2$ takes place. Nevertheless, spectral changes are visible for the high frequency peak, which forms a shoulder at higher IL concentration. A closer look at the IL region of the spectra helps to understand these changes. Apart from the expected peaks at 1265, 1226, 1156 and 1036 cm^{-1}, which were observed previously, additional weaker features form at 1203 and 1015 cm^{-1} over time. We attribute this behavior to ligand exchange with the $[OTf]^-$ anions themselves. In previous work it was already reported that in DCM solution Cl^- at the Ru^{II} metal center can be substituted by $[OTf]^-$ ligands.[27] Although the amount of $[OTf]^-$-species in this previous study was very low (~1%), the authors could obtain a crystal structure of this complex.

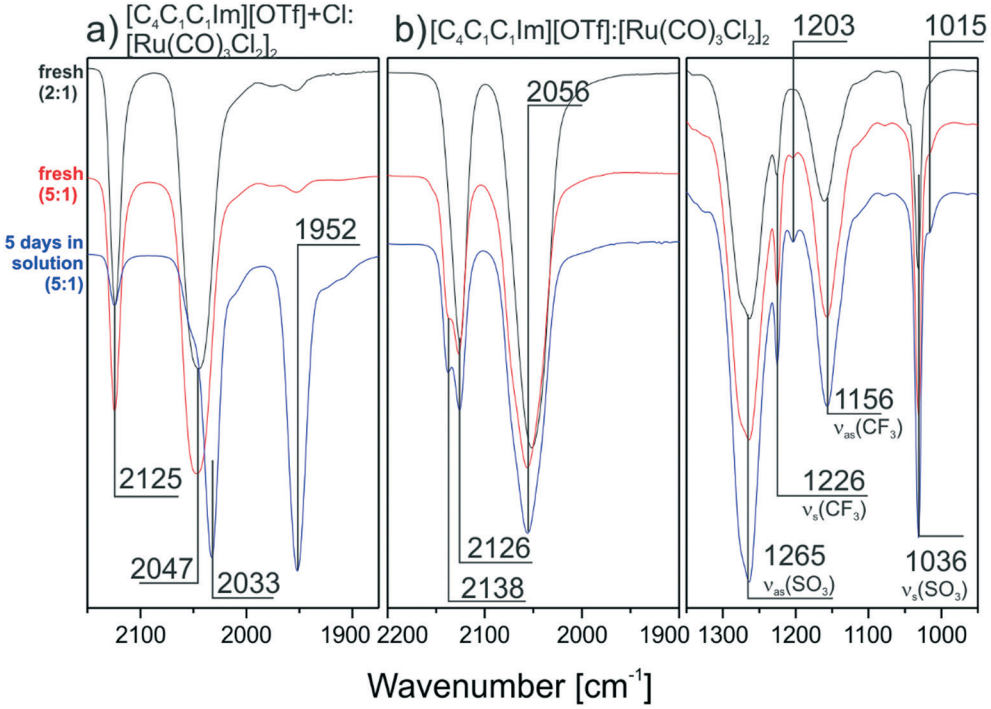

Fig. 3 Offset and normalized reference TIRS spectra for a) $[Ru(CO)_3Cl_2]_2/[C_4C_1C_1Im]Cl/[OTf]$ mixture and b) $[Ru(CO)_3Cl_2]_2/[C_4C_1C_1Im][OTf]$ mixtures (IL region included) both prepared with DCM.

Moreover, we were able to spectroscopically identify $[OTf]^-$ bound in a ligand-like fashion to a metal support in recent ultra-high vacuum studies with 1-ethyl-2-methylimidazolium trifluoromethanesulfonate ($[C_2C_1Im][OTf]$).[28] In the $[C_2C_1Im]$-[OTf] monolayer, the anions interact with a Pd support *via* the SO_3-group, leading to red-shifted ν_s(S–O) and ν_{as}(S–O) signals at ~1010 and 1216 cm^{-1}, respectively. Similar features located at 1204 and 1016 cm^{-1} can also be found in the TIR spectra recorded from $[C_4C_1C_1Im][OTf]:[Ru(CO)_3Cl_2]_2$ mixtures as seen in the spectrum recorded after 5 days. The band intensity of the $[OTf]^-$ ligand species is lower compared to its solvent counterpart, but its temporal evolution shows that the concentration of the $Ru^{II}[OTf]^-$ complex increases with time.

Our findings support the assumption that there is a slow time- and concentration-dependent conversion of $[Ru(CO)_3Cl_2]_2$ to a series of different monomers driven by Cl^- from the supporting IL phase. The major species on the freshly prepared SILP catalyst using $[Ru(CO)_3Cl_2]_2$ as a precursor is $[Ru(CO)_3Cl_3]^-$. In addition, we find species with a larger number of Cl^- ligands, formed at lower concentration. The formation and the nature of the $[Ru(CO)_xCl_y]_n$ species clearly depends strongly on the concentration of Cl^- ions. It is expected that the speciation should have a direct influence on the catalytic properties of the SILP system.

3.2. Influence of Cl^--content on overall catalytic behavior of the SILP system

To ascertain the dependence of speciation and catalytic activity on the Cl^- concentration, a series of experiments with different sources and concentration of Cl^- was performed. Apart from $[C_4C_1C_1Im]Cl$, NaCl was also chosen as the Cl^- source. All catalysts were prepared from $[Ru(CO)_3Cl_2]_2$ as described in the experimental section, except that the additional Cl^- source was dissolved in DCM as well. The water content (20 vol%) under experimental conditions enhances NaCl dissolution. Details on the apparatus used to conduct the activity measurements can be found in the ESI.† Specifically, the investigated systems were (from low to high Cl^- content): $[C_4C_1C_1Im][OTf]$, a mixture of $[C_4C_1C_1Im][OTf]$ doped with $[C_4C_1C_1Im]Cl$ (equal volume with respect to the pore filling ratio of $\alpha = 0.34$), $[C_4C_1C_1Im][OTf]$ doped with NaCl (equimolar), $[C_4C_1C_1Im]Cl$ as the benchmark system and an equimolar mixture of $[C_4C_1C_1Im]Cl$ and NaCl. In Table 2 we summarize the activity given as the maximum turn over frequency (TOF_{140}, $mol_{CO2}mol_{Ru}^{-1}$ h^{-1} at 140 °C and steady) and the Cl^- concentration given as molar fraction of the complete mixture normalized to the benchmark. Furthermore, the Cl^--source other than experimentally induced by the precursor is given. The experiments show that at low concentration, Cl^- has a positive effect on the catalytic performance. A certain fraction of Cl^- ($x_{Cl} = 0.31$) is present in each of the above-mentioned systems. This fraction originates from the precursor complex, which contains Cl^- as well (see $[C_4C_1C_1Im][OTf]$ with $x_{Cl} = 0.31$). By comparison of the $[C_4C_1C_1Im][OTf]$ system (TOF = 26.1 h^{-1}, $x_{Cl} = 0.31$) with the NaCl doped equivalent (TOF = 33.8 h^{-1}, $x_{Cl} = 0.84$), a relative increase in performance of 29.5% is observed, which supports the assumption that Cl^- ions enhance the WGSR by the formation of different Cl^--rich monomers, starting from the $[Ru(CO)_3Cl_2]_2$ dimer. The

Table 2 Summary of the series of experiments varying the chloride concentration

IL	Cl^--source[a]	$x(Cl^-)$[a] [—]	TOF [h^{-1}]
$[C_4C_1C_1Im][OTf]$	—	0.31	26.1
$[C_4C_1C_1Im][OTf]$ + $[C_4C_1C_1Im]Cl$	$[C_4C_1C_1Im]Cl$	0.66	61.4
$[C_4C_1C_1Im][OTf]$ + NaCl	NaCl	0.84	33.8
$[C_4C_1C_1Im]Cl$	$[C_4C_1C_1Im]Cl$	1.00	72.5
$[C_4C_1C_1Im]Cl$ + NaCl	$[C_4C_1C_1Im]Cl$ + NaCl	1.70	61.2

[a] Other than experimentally induced Cl^- source respectively Cl^- content by precursor.

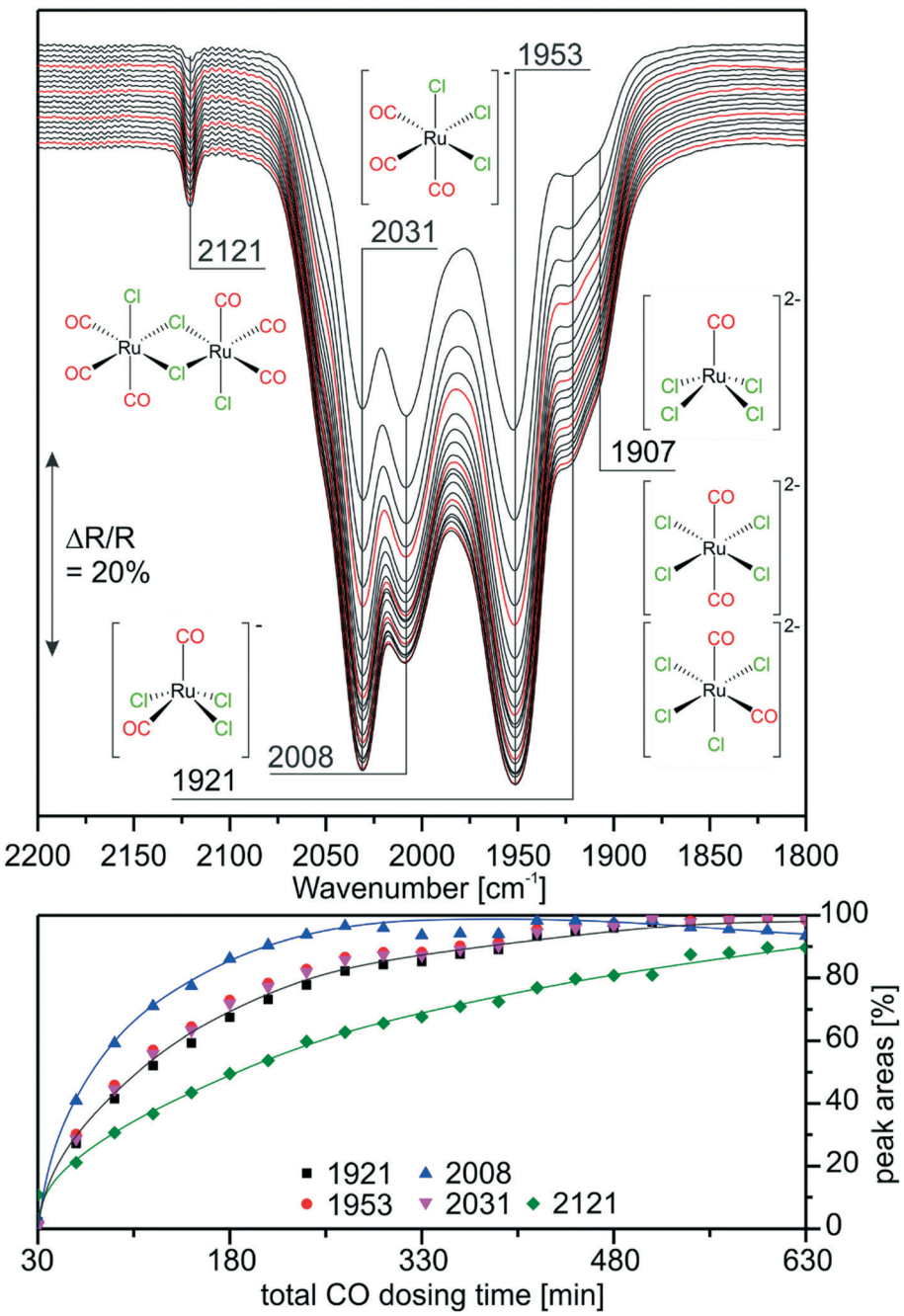

Fig. 4 Top: Offset DRIFT spectra taken during CO treatment on $RuCl_3/[C_4C_1C_1Im]Cl/Al_2O_3$. Each spectrum is taken after the respective cycle of 30 min CO dosing, a subsequent 1 min evacuation and 15 min Ar purge; bottom: integrated, normalized and averaged (over the complete Ar purging time) peak areas (all lines are guides to the eye).

effect becomes even more visible when comparing $[C_4C_1C_1Im][OTf]$ with the $[C_4C_1C_1Im][OTf]$/Cl mixture (TOF = 61.4 h^{-1}, x_{Cl} = 0.66, α_i = 0.17; α_{tot} = 0.34; $n_{[C4C1C1Im][OTf]}$: $n_{[C4C1C1Im]Cl}$ = 1 : 1.3). A boost in performance of more than 230% is achieved by doubling the Cl^--content. The large change in performance resulting from a relatively small increase in Cl^- content suggests that the counter ion of the doping agent plays an important role as well. This assumption is supported by comparing the $[C_4C_1C_1Im]Cl$ benchmark system (TOF = 72.5 h^{-1}, x_{Cl} = 1.00) with the NaCl-doped equivalent (TOF = 33.8 h^{-1}, x_{Cl} = 0.84), where a decrease in performance by 53,3% can be observed. Additionally, a comparison between the $[C_4C_1C_1Im]Cl$ benchmark system (TOF = 72.5 h^{-1}, x_{Cl} = 1.00) with the NaCl doped benchmark system shows a decrease in performance of 15,5%, in spite of the fact that an increase of the activity would be expected due to the higher Cl^- content. These results indicate that Na^+ as counter ion has a hindering effect as compared to $[C_4C_1C_1Im]^+$. In addition, NaCl may form solid precipitates in the pores of the support leading to partial blocking of the pores.

The Ru-carbonyls identified so far can be interconverted simply by consecutive Cl^-/CO ligand substitutions, therefore we conclude that an equilibrium is established between the various observed species during the catalytic reaction.

3.3. Carbonylation of $RuCl_3$

As mentioned earlier, previous experiments suggested that $[Ru(CO)_xCl_y]_n$ species are also produced from $RuCl_3$ under WGSR conditions in a SILP system.[9] In order to prove that similar species are formed on the $RuCl_3$- and $[Ru(CO)_3Cl_2]_2$-based catalysts we monitored the carbonylation of $RuCl_3$/$[C_4C_1C_1Im]Cl/Al_2O_3$ by *in situ* IR spectroscopy. As described in the experimental section, CO was dosed in steps interrupted by purging periods, to be able to resolve also those peaks which are otherwise hidden by the gas-phase CO bands. Fig. 4 shows the last spectrum recorded in purge mode for each CO dosing step. We observe the same bands as in the reference experiments discussed above. After short CO exposure, the spectra show prominent features at 2031 and 1953 cm^{-1}, indicating that the major species in the $RuCl_3$-based system is again $[Ru(CO)_3Cl_3]^-$. The occurrence of a small peak at 1907 cm^{-1} indicates that the di-anionic species $[Ru(CO)_2Cl_4]^{2-}$ or $[RuCOCl_4]^{2-}$ is also formed in lower concentrations. Interestingly, the feature of $[Ru(CO)_2Cl_3]^-$ at 2008 cm^{-1} is quite intense at the early stages of CO dosing. Indeed, it is almost as intense as the peaks of $[Ru(CO)_3Cl_3]^-$. This is probably due to the fact that $[Ru(CO)_2Cl_3]^-$ is one of the first carbonylation products formed from $RuCl_3$ by addition of two CO ligands. In fact, the amount of $[Ru(CO)_2Cl_3]^-$ decreases at later stages of the experiment indicating its consumption by a consecutive reaction. This temporal behavior supports our previous assignment of the peak.

The sharp feature at 2121 cm^{-1} which corresponds to the $[Ru(CO)_3Cl_2]_2$ dimer is quite small and increases in intensity more slowly. Previous results with the $[Ru(CO)_3Cl_2]_2$/$[C_4C_1C_1Im]Cl/Al_2O_3$ system suggested the formation of monomers, thus, the back-reaction and formation of $[Ru(CO)_3Cl_2]_2$ in the IL is implausible. One possible explanation is that no dimerization takes place, but the $[Ru(CO)_3Cl_2]$ monomer is formed in small amounts. The calculated spectrum of square pyramidal (s.-pyr.) *cis*-$[Ru(CO)_3Cl_2]$ strongly resembles the spectrum of the dimer. Although unambiguous assignment of the bands at 2121 and 2155 cm^{-1} may, therefore, not be possible, it is clear that upon CO dosing several of the previously identified Ru-carbonyls are formed. Similar species like $[Ru(CO)_3Cl_2]_2$, *fac*-$[Ru(CO)_3Cl_3]^-$ and $[Ru(CO)_2Cl_4]^{2-}$ were also found during carbonylation of $RuCl_3$ in refluxing ethanol/ethoxyethanol.[29,30] Thus, freshly prepared $[Ru(CO)_3Cl_2]_2$ (in the presence of Cl^-) and carbonylated $RuCl_3$ SILP catalysts exhibit similar Ru-species, mostly $[Ru(CO)_3Cl_3]^-$. In the case of $RuCl_3/[C_4C_1C_1Im]Cl/Al_2O_3$ such carbonylated species can only be formed under reaction conditions. This explains the induction period observed in the catalytic activity.[9] The new results indicate that CO dosing at ambient conditions (1 bar, RT) should give rise to a similar effect as preparation of the SILP catalyst with $[Ru(CO)_3Cl_2]_2$. This finding is interesting from an economic point of view, as $RuCl_3$ is a cheaper starting material than $[Ru(CO)_3Cl_2]_2$.

In the next step, we tested the response of the carbonylated $RuCl_3/[C_4C_1C_1Im]Cl/Al_2O_3$ system to a change in temperature. The experiments were performed in Ar atmosphere at 1 bar. A summary of the results is displayed in Fig. 5. Upon heating above 75 °C, the peak at 2121 cm^{-1} decreases in intensity until no band is visible anymore above 125 °C. Simultaneously, a peak with increasing intensity is observed at 1902 cm^{-1}. This points to the formation of chlorine-rich Ru-carbonyls from CO-rich species. The loss of CO ligands is expected, as carbonylchlororuthenium complexes like $[Ru(CO)_3Cl_2]_2$ are frequently used as CO releasing molecules (CO-RM) in, for example, medical applications.[31] It was reported that up to 0.7 mole CO per mole $[Ru(CO)_3Cl_2]_2$ can be released in DMSO.[26] As both peaks of $[Ru(CO)_2Cl_3]^-$ appear rather as shoulders, it cannot be clearly deduced whether this species increases in intensity or the signal is suppressed by the increase of the more dominant features of $[Ru(CO)_3Cl_3]^-$ at 2032 cm^{-1} and $[Ru(CO)_2Cl_4]^{2-}$ or $[RuCOCl_4]^{2-}$ at 1902 cm^{-1}. Moreover, a new peak is formed at 1735 cm^{-1} upon heating which was not observed before. Our DFT calculations (see ESI†) suggest that features at such low wavenumbers are found only for carbonyl–carboxylate complexes and five-coordinated Ru^0 carbonyls in trigonal-bipyramidal (trig.-bip.) configuration (see Table 1). The formation of a Ru^0 species is relatively unlikely under the present conditions (see also section 3.5). The formation of carboxylates could result from the presence of water in the system, which we consider as unlikely or, potentially, from OH species arising from the Al_2O_3 support. However, formation of a carboxylate from one CO ligand species should influence the carbonyl peaks at higher wavenumbers, which is not observed. The definite assignment of this peak is, therefore, not possible at the present time.

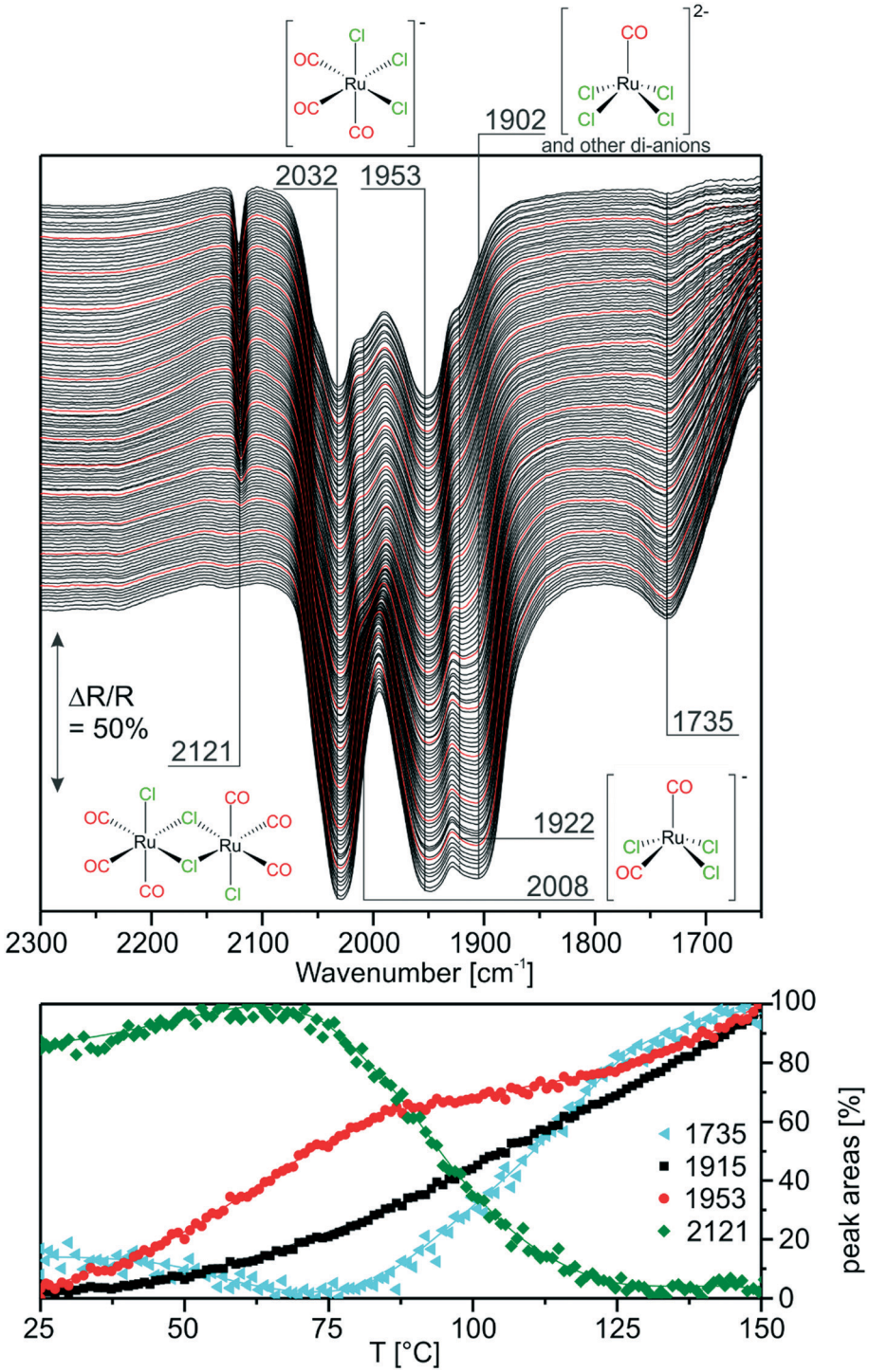

Fig. 5 Top: Offset DRIFT spectra during heating the carbonylated $RuCl_3/[C_4C_1C_1Im]Cl/Al_2O_3$ sample; bottom: selected, normalized peak areas (all lines are guides to the eye).

In general, we observe that only little peak intensity is lost while, at the same time, several peaks drastically increase in intensity. One explanation for this observation is that upon heating IL and Ru species diffuse in the porous system and – at the applied high IL loading – even some may diffuse out of the pores of the support. The change in peak intensity of the IL-related peaks, which should increase correspondingly, supports this hypothesis (see ESI†). In addition residual $RuCl_3$ species in the catalyst pellets may react with CO and form additional $[Ru(CO)_3Cl_3]^-$, which would also lead to an increase in the intensity of the respective features.

The experiments with $RuCl_3/[C_4C_1C_1Im]Cl/Al_2O_3$ confirm that an equilibrium is established between different

$[Ru(CO)_xCl_y]_n$ species present in the two SILP systems that are active for WGSR.

3.4. Carbonylation of $[Ru(CO)_3Cl_2]_2/[C_4C_1C_1Im]Cl/Al_2O_3$

With the above findings, we now return to the initially investigated $[Ru(CO)_3Cl_2]_2/[C_4C_1C_1Im]Cl/Al_2O_3$ system and its response to CO dosing. In Fig. 6, the spectra obtained during CO dosing on $[Ru(CO)_3Cl_2]_2/[C_4C_1C_1Im]Cl/Al_2O_3$ are shown over a total duration of 360 min. As the background spectrum was taken before starting the experiment, peaks pointing upwards correspond to loss of intensity or decrease of the respective species, whereas peaks pointing downwards show the formation of the corresponding species. In line with results presented above, we assume that the major species in the examined sample is $[Ru(CO)_3Cl_3]^-$ with a smaller amount of $[Ru(CO)_2Cl_3]^-$ and chloride-rich species such as $[Ru(CO)_2Cl_4]^{2-}$ or $[RuCOCl_4]^{2-}$ also being present. Upon CO dosing, we observe the loss of peak intensity around 1900 cm^{-1}, a spectral region attributed to the latter chloride-rich

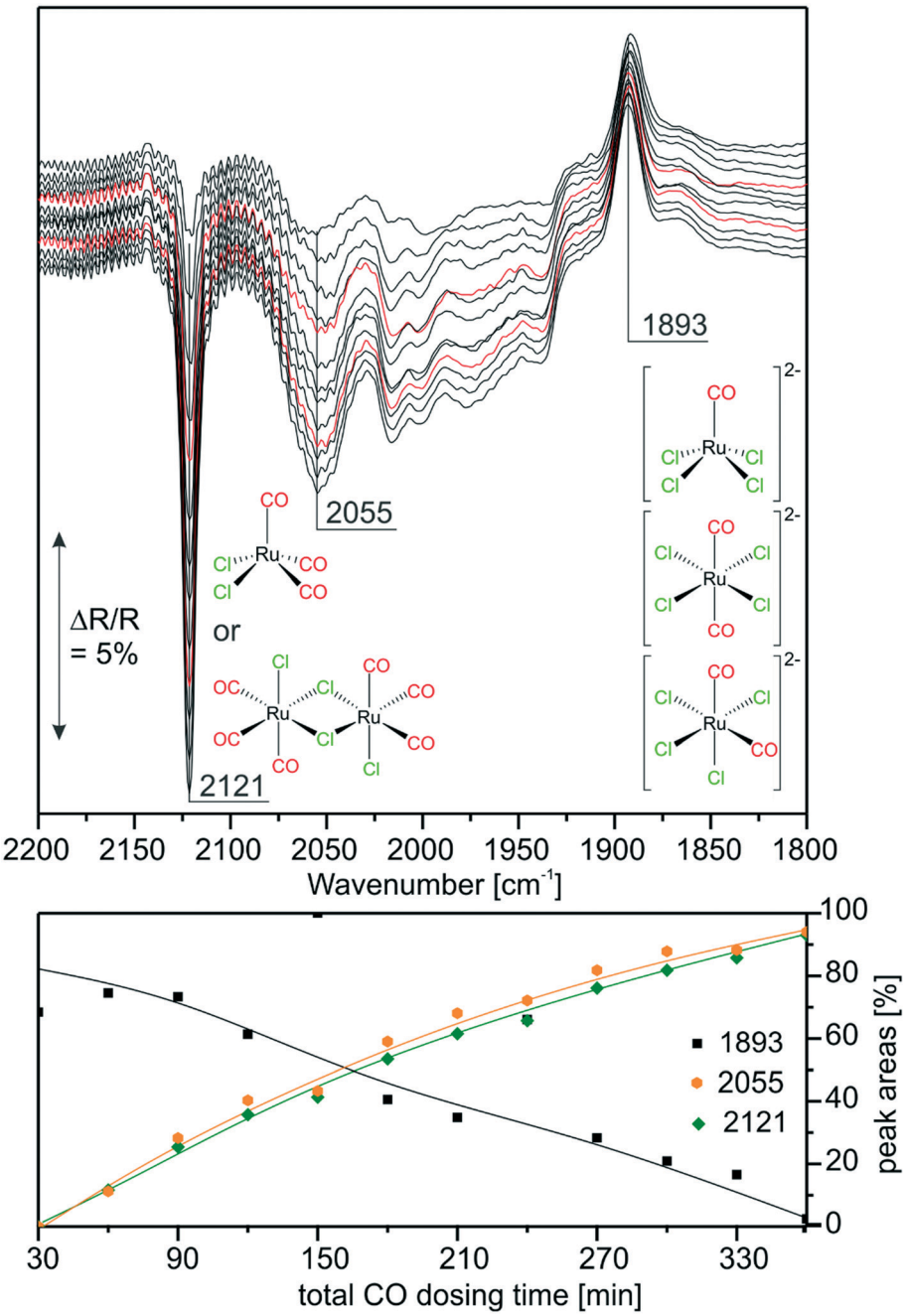

Fig. 6 Top: Offset DRIFT spectra taken during CO treatment on the as-obtained SILP catalyst, each spectrum is taken after the respective cycle of 30 min CO dosing, a subsequent 1 min evacuation and 15 min Ar purge step (to remove the CO gas phase from the reactor); bottom: integrated, normalized peak areas (all lines are guides to the eye).

complexes. The decrease is linear throughout the experiment, and is accompanied by an increase in intensity of the peaks at 2121 and 2055 cm^{-1}, which are assigned to $[Ru(CO)_3Cl_2]$ or $[Ru(CO)_3Cl_2]_2$. This shows that the equilibrium is shifted towards complexes containing more CO ligands. The peak at 2055 cm^{-1} is quite small, which can be explained by the fact that strong absorption of $[Ru(CO)_3Cl_3]^-$ around 2030 cm^{-1} leads to a decrease in sensitivity compared to the spectral region around 2121 cm^{-1}. Thus, the peak at 2055 cm^{-1} observed in the difference spectra appears to be less intense. We suggest that in the case of five coordinated Ru complexes the observed ligand substitution occurs in an associative fashion *via* a six-fold coordinated 18 valence electron transition state.

Upon CO dosing the amount of chloride-rich species decreases and $[Ru(CO)_3Cl_2]$ or $[Ru(CO)_3Cl_2]_2$ species are formed

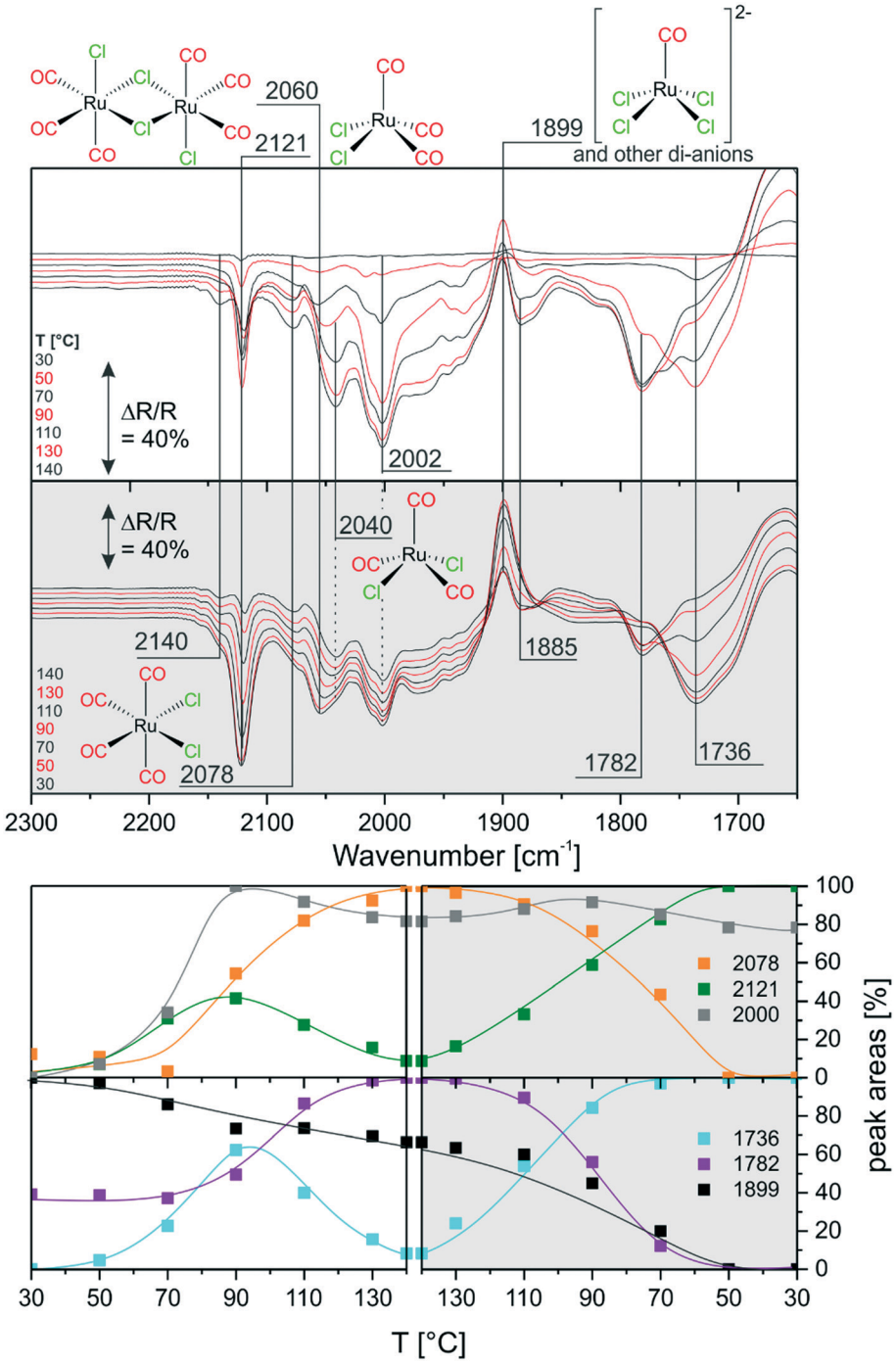

Fig. 7 Top: Offset DRIFT spectra taken during CO treatment upon heating on the as-obtained SILP catalyst, each spectrum is taken after a cycle of 30 min CO dosing, a subsequent 1 min evacuation and 15 min Ar purge (the two latter steps remove the CO gas phase from the reactor) at the respective temperature; bottom: integrated, normalized peak areas (all lines are guides to the eye).

with more CO ligands bound to the Ru metal center. This observation supports the presence of a dynamic equilibrium between these species.

3.5. Carbonylation of $[Ru(CO)_3Cl_2]_2$/$[C_4C_1C_1Im]Cl/Al_2O_3$ at elevated temperatures

Next, we investigated the carbonylation at elevated temperatures from 30 to 140 °C. Fig. 7 shows the difference spectra recorded in Ar purge mode after CO dosing at each temperature step. We observe that the feature related to chloride-rich species at ~1899 cm^{-1} decreases in intensity. These complexes undergo carbonylation to form the previously discussed (s.-pyr. *cis*-) $[Ru(CO)_3Cl_2]$ or dimer species as indicated by the peaks at 2121 and 2060 cm^{-1}. The overall increasing intensity of positive and negative peaks in the spectra with respect to the isothermal CO dosing experiment at RT indicates that, at elevated temperatures, the conversion to CO-rich species is enhanced. Moreover, new species can be identified. For example the two rather broad features at 2040 and 2002 cm^{-1} can be assigned to the s.-pyr. *trans*-$[Ru(CO)_3Cl_2]$ monomer, which is less stable compared to the *cis* conformer. As the band at 2040 cm^{-1} lies in between two intense features at 2060 cm^{-1} and 2030 cm^{-1} ($[Ru(CO)_3Cl_3]^-$), its quantification is difficult. Therefore, Fig. 7 only includes integrated and normalized areas of the peak at 2002 cm^{-1}. The amount of s.-pyr. *trans*-$[Ru(CO)_3Cl_2]$ (grey curve) increases quickly upon heating and CO dosing and it appears to be stable in CO atmosphere also during the cooling period. The behavior of the integrated peak areas of all observed $[Ru(CO)_3Cl_2]$ monomer (s.-pry., *cis*/*trans*) and dimer complexes shows interconversion between the different isomers. At high temperatures, the less stable s.-pyr. *trans* structure is favored.

A closer look at the spectra reveals that a small feature at 2140 cm^{-1} in combination with a band at 2078 cm^{-1} (orange curve) develops at temperatures above ~80 °C. As peaks located at such high wavenumbers point to CO-rich Ru-complexes, this signal pair can be assigned to $[Ru(CO)_4Cl_2]$.[32] The third peak expected from DFT at ~2030 cm^{-1} coincides with bands from other species and, therefore, cannot easily be identified in the spectra. $[Ru(CO)_4Cl_2]$ may indeed be formed from $[Ru(CO)_3Cl_2]$ or the corresponding dimer in either configuration by carbonylation. It is stable above 90 °C in our experiment, whereas decreasing peaks areas of the $[Ru(CO)_3Cl_2]$ conformers or dimer (green and grey curve) indicate consumption of the latter at high temperatures.

During cooling, $[Ru(CO)_4Cl_2]$ re-converts to $[Ru(CO)_3Cl_2]$ or $[Ru(CO)_3Cl_2]_2$ complexes by loss of CO. The amount of s.-pyr. *trans*-$[Ru(CO)_3Cl_2]$ at 2002 cm^{-1} decreases upon cooling, although the process seems not to be completed on the time scale of the present experiment.

Furthermore, the spectral region at lower wavenumbers shows an interesting behavior. Firstly, the peak at 1736 cm^{-1} develops upon heating, as expected from the heating experiment of carbonylated $RuCl_3$. Secondly, the peak intensity decreases above 90 °C and a new peak at 1782 cm^{-1} is formed at the same time. The cooling ramp shows that this behavior is reversible. As discussed above the corresponding bands may be attributed to carbonyl–carboxylate or Ru^0 species. We tentatively assign the low frequency peaks to carbonyl–carboxylate species formed with OH species from the Al_2O_3 support, as both the appreciable presence of water and reversible formation of Ru^0 carbonyl species seem quite unlikely.

In the context of CO dosing, the question arises whether full carbonylation to $Ru_3(CO)_{12}$ is possible under the present conditions. The infrared spectrum of $Ru_3(CO)_{12}$ on Al_2O_3 shows a broad vibrational structure between 1900 and 2100 cm^{-1}.[32] On one hand, this could explain the broad smeared-out structure, which develops upon heating exactly in this spectral region. On the other hand, it has been reported that the presence of halide anions readily leads to CO displacement in $Ru_3(CO)_{12}$, especially in solvents which increase the nucleophilicity of Cl^-.[33] Still, these experiments have not been conducted in CO atmosphere.

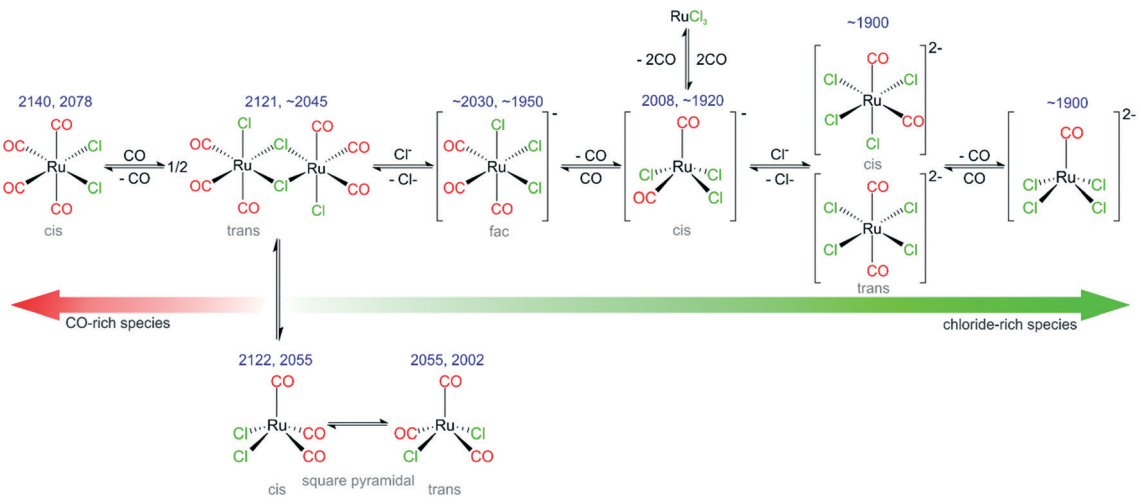

Fig. 8 Overview of Ru complexes observed during the investigation of the different SILP systems and reference experiments. Peak positions taken from the measurements are included. Note that for the sake of clarity not all possible ligand exchange reactions are indicated.

In comparison with the CO dosing experiments performed at RT we conclude that at elevated temperatures carbonylation of chloride-rich species is possible even up to formation of $[Ru(CO)_4Cl_2]$. This species was previously not observed in the presented experiments and seems to be associated with appreciable concentration only at temperatures above 80 °C.

4. Conclusion

In this work, using a combination of DRIFTS and DFT, we investigated $[Ru(CO)_xCl_y]_n$ based SILP catalysts, which are active for the low-temperature WGSR. From our results we are able to draw the following conclusions:

1) It is shown that the $[Ru(CO)_xCl_y]_n$ SILP is a dynamic system, with a speciation that responds to the reaction conditions. In particular, we investigated the role of the reaction temperature and the CO pressure.

2) With the help of DFT calculations, several species that are present under reaction conditions have been identified. Their nature is summarized in Fig. 8. Specifically, we identify the following species: *fac*-$[Ru(CO)_3Cl_3]^-$ (major species in the freshly prepared catalyst), *cis*-$[Ru(CO)_2Cl_3]^-$, *cis*-/*trans*-$[Ru(CO)_2Cl_4]^{2-}$, $[Ru(CO)Cl_4]^{2-}$, s.-pyr. *cis*-/*trans*-$[Ru(CO)_3Cl_2]$ and *cis*-$[Ru(CO)_4Cl_2]$.

3) Successive elimination/addition steps lead to principle groups of intermediates. In this reaction sequence, the applied chloride IL acts as an effectively infinite reservoir of chloride ligands.

4) Upon preparation of $[Ru(CO)_3Cl_2]_2/[C_4C_1C_1Im]Cl/Al_2O_3$ by impregnation in DCM, the Ru dimer splits and a $[Ru(CO)_3Cl_3]^-$ monomer is formed, together with a small amount of $[Ru(CO)_2Cl_3]^-$, $[Ru(CO)_2Cl_4]^{2-}$ and $[RuCOCl_4]^{2-}$.

5) The same species are found, if the catalyst is prepared from $RuCl_3/[C_4C_1C_1Im]Cl/Al_2O_3$ followed by subsequent CO dosing at room temperature.

6) Heating leads to CO release and an increasing fraction of chloride-rich di-anionic species (right-hand side in Fig. 8), whereas CO dosing drives the equilibrium to the CO-rich (left-hand) side. CO dosing at elevated temperatures enhances this transformation and leads even to formation of CO-rich species such as $[Ru(CO)_4Cl_2]$.

7) In addition to Ru-complexes with varying numbers of Cl^- and CO ligands, different conformers of the $[Ru(CO)_3Cl_2]$ monomer have been identified. Some of the species observed are present only at elevated temperatures in CO atmosphere.

8) The beneficial effect of Cl^- addition on the equilibria between different Ru-chloro-carbonyl species is also reflected in the catalytic activity. Higher Cl^- concentrations in the IL layer result in more active WGS catalysts.

The presented experiments show that a variety of Ru-complexes can be identified by *in situ* DRIFTS in combination with DFT. Further experiments are planned involving the influence of water in operando mode. In this way, it should be feasible to assign catalytic activities in an even more reliable fashion.

Conflicts of interest

There are no conflicts to declare.

Acknowledgements

The authors gratefully acknowledge funding by the German Research Council (DFG), which, within the framework of its "Excellence Initiative" supports the Excellence Cluster "Engineering of Advanced Materials" (www.eam.fau.de) at the Friedrich-Alexander-Universität Erlangen-Nürnberg" (project EXC 315) (Bridge Funding). T. B. gratefully acknowledges financial support from the "Fonds der Chemischen Industrie". R. S., C. W., A.-S. S. and D. M. S. acknowledge the DAAD project Multiscale Modelling of Supported Ionic Liquid Phase Catalysis (2017–2018), as well as the NIS project 11311 at the Juelich Supercomputing facilities. P. Wa., M. H. and P. Wo. gratefully acknowledges financial support from the European Commission within the Horizon 2020-SPIRE project ROMEO (grand agreement number 680395).

References

1 S. R. J. Byron, L. Muruganandam and S. M. Shekhar, *Int. J. Chem. React. Eng.*, 2010, **8**, DOI: 10.2202/1542-6580.2238.
2 M. H. Halabi, M. H. J. M. de Croon, J. van der Schaaf, P. D. Cobden and J. C. Schouten, *Appl. Catal., A*, 2010, **389**, 68–79.
3 J. D. Holladay, J. Hu, D. L. King and Y. Wang, *Catal. Today*, 2009, **139**, 244–260.
4 G. Jacobs and B. H. Davis, in *Catalysis: Volume 20*, The Royal Society of Chemistry, 2007, vol. 20, pp. 122–285.
5 S. Werner, N. Szesni, R. W. Fischer, M. Haumann and P. Wasserscheid, *Phys. Chem. Chem. Phys.*, 2009, **11**, 10817–10819.
6 A. Riisager, R. Fehrmann, M. Haumann and P. Wasserscheid, *Eur. J. Inorg. Chem.*, 2006, 695–706, DOI: 10.1002/ejic.200500872.
7 C. P. Mehnert, *Chem. – Eur. J.*, 2004, **11**, 50–56.
8 H. P. Steinrück, J. Libuda, P. Wasserscheid, T. Cremer, C. Kolbeck, M. Laurin, F. Maier, M. Sobota, P. S. Schulz and M. Stark, *Adv. Mater.*, 2011, **23**, 2571–2587.
9 S. Werner, N. Szesni, A. Bittermann, M. J. Schneider, P. Härter, M. Haumann and P. Wasserscheid, *Appl. Catal., A*, 2010, **377**, 70–75.
10 S. Werner, N. Szesni, M. Kaiser, R. W. Fischer, M. Haumann and P. Wasserscheid, *ChemCatChem*, 2010, **2**, 1399–1402.
11 J. M. Butler, M. W. George, J. R. Schoonover, D. M. Dattelbaum and T. J. Meyer, *Coord. Chem. Rev.*, 2007, **251**, 492–514.
12 T. Bauer, V. Hager, M. Williams, M. Laurin, T. Döpper, A. Görling, N. Szesni, P. Wasserscheid, M. Haumann and J. Libuda, *ChemCatChem*, 2017, **9**, 109–133.
13 *TURBOMOLE V6.6 2014*, a development of University of Karlsruhe and Forschungszentrum Karlsruhe GmbH, 1989-2007, TURBOMOLE GmbH, since 2007; available from http://www.turbomole.com.
14 R. Ahlrichs, M. Bar, M. Haser, H. Horn and C. Kolmel, *Chem. Phys. Lett.*, 1989, **162**, 165–169.
15 A. D. Becke, *Phys. Rev. A: At., Mol., Opt. Phys.*, 1988, **38**, 3098–3100.

16 J. P. Perdew, *Phys. Rev. B: Condens. Matter Mater. Phys.*, 1986, **33**, 8822–8824.
17 F. Weigend and R. Ahlrichs, *Phys. Chem. Chem. Phys.*, 2005, **7**, 3297–3305.
18 R. A. Kendall, T. H. Dunning and R. J. Harrison, *J. Chem. Phys.*, 1992, **96**, 6796–6806.
19 D. E. Woon and T. H. Dunning, *J. Chem. Phys.*, 1993, **98**, 1358–1371.
20 M. Sobota, S. Schernich, H. Schulz, W. Hieringer, N. Paape, P. Wasserscheid, A. Görling, M. Laurin and J. Libuda, *Phys. Chem. Chem. Phys.*, 2012, **14**, 10603–10612.
21 M. Kaltchev and W. T. Tysoe, *Surf. Sci.*, 1999, **430**, 29–36.
22 B. Haddad, D. Mokhtar, M. Goussem, E.-H. Belarbi, D. Villemin, S. Bresson, M. Rahmouni, N. R. Dhumal, H. J. Kim and J. Kiefer, *J. Mol. Struct.*, 2017, **1134**, 582–590.
23 L. Huang and Y. Xu, *J. Mol. Catal. A: Chem.*, 2001, **176**, 267–280.
24 D. Roberto, R. Psaro and R. Ugo, *Organometallics*, 1993, **12**, 2292–2296.
25 K. Tsuchiya, J.-D. Huang and K.-i. Tominaga, *ACS Catal.*, 2013, **3**, 2865–2868.
26 R. Motterlini, J. E. Clark, R. Foresti, P. Sarathchandra, B. E. Mann and C. J. Green, *Circ. Res.*, 2002, **90**, E17–24.
27 G. Santiso-Quinones and R. E. Rodriguez-Lugo, *Acta Crystallogr., Sect. C: Cryst. Struct. Commun.*, 2013, **69**, 859–861.
28 T. Bauer, S. Mehl, O. Brummel, K. Pohako-Esko, P. Wasserscheid and J. Libuda, *J. Phys. Chem. C*, 2016, **120**, 4453–4465.
29 M. L. Berch and A. Davidson, *J. Inorg. Nucl. Chem.*, 1973, **35**, 3763–3767.
30 N. Lugan, G. Lavigne, J. M. Soulie, S. Fabre, P. Kalck, J. Y. Saillard and J. F. Halet, *Organometallics*, 1995, **14**, 1712–1731.
31 A. A. Ahanger, S. Prawez, D. Kumar, R. Prasad, Amarpal, S. K. Tandan and D. Kumar, *Naunyn-Schmiedeberg's Arch. Pharmacol.*, 2011, **384**, 93–102.
32 V. L. Kuznetsov, A. T. Bell and Y. I. Yermakov, *J. Catal.*, 1980, **65**, 374–389.
33 J. Lillis, A. Rokicki, T. Chin and P. C. Ford, *Inorg. Chem.*, 1993, **32**, 5040–5043.